MAJOR ARTICLE

Pathologic Changes in Mice Induced by Subtilase Cytotoxin, a Potent New *Escherichia coli* AB_5 Toxin That Targets the Endoplasmic Reticulum

Hui Wang, James C. Paton, and Adrienne W. Paton

School of Molecular and Biomedical Science, University of Adelaide, Australia

Subtilase cytotoxin (SubAB) is the prototype of a recently discovered AB_5 cytotoxin family produced by certain strains of Shiga toxigenic *Escherichia coli* (STEC). The catalytic A subunit is a highly specific subtilase-like serine protease that cleaves the endoplasmic reticulum chaperone BiP. The toxin is lethal for mice, but the pathology it induces is poorly understood. Here, we show that intraperitoneal injection of SubAB causes microangiopathic hemolytic anemia, thrombocytopenia, and renal impairment in mice—characteristics typical of Shiga toxin–induced hemolytic uremic syndrome. SubAB caused extensive microvascular thrombosis and other histologic damage in the brain, kidneys, and liver, as well as dramatic splenic atrophy. Peripheral blood leukocyte levels were increased at 24 h; there was also significant neutrophil infiltration in the liver, kidneys, and spleen and toxin-induced apoptosis at these sites. These findings raise the possibility that SubAB directly contributes to pathology in humans infected with strains of STEC that produce both Shiga toxin and SubAB.

Shiga toxigenic *Escherichia coli* (STEC) produce AB_5 toxins belonging to the Shiga toxin (Stx) family [1, 2]. Their pentameric B subunits bind glycolipid receptors on target cells. This is followed by internalization of the toxin, retrograde transport to the endoplasmic reticulum (ER), translocation of the A subunit into the cytoplasm, and inhibition of protein synthesis. STEC cause severe gastrointestinal disease in humans that may result in hemorrhagic colitis (HC) and hemolytic uremic syndrome (HUS; a triad of microangiopathic hemolytic anemia, thrombocytopenia, and renal failure) [1, 2]. The pathology of severe STEC disease is considered to be directly attributable to Stx. STEC colonize the gut, and Stx released into the lumen is translocated across the intestinal epithelium and absorbed into the circulation. It then targets tissues expressing the receptor Gb_3, which in humans is found in highest concentrations in renal tubular epithelial cells and in microvascular endothelial cells, particularly in the kidneys, gut, and brain. Stx-mediated damage at these sites is consistent with the pathology of HUS. Microvascular and concomitant ischemic damage to the intestinal wall also accounts for the severe bloody diarrhea associated with HC [1, 2].

There is increasing evidence that STEC strains vary in their capacity to cause serious disease. A contributing factor may be the amount or subtype of Stx produced. However, molecular investigations have identified potential accessory virulence factors encoded on pathogenicity islands or plasmids [1, 2]. One such factor is the capacity to produce attaching/effacing lesions on enterocytes, encoded by the locus for enterocyte effacement (LEE) [2]. LEE-positive STEC cause most cases of HUS, particularly in outbreak settings [1, 2]. However, in 1998 we investigated a small outbreak of HUS caused by an O113:H21 STEC that produced Stx2 but was LEE negative [3]. Despite the absence of LEE, O113:H21 STEC are highly virulent, causing disease at the extreme end of the clinical spectrum. O113:H21

Received 5 February 2007; accepted 8 May 2007; electronically published 22 August 2007.

Potential conflicts of interest: none reported.

Financial support: National Health and Medical Research Council of Australia (program grant 284214); National Institutes of Health (grant RAI068715A).

Reprints or correspondence: Dr. Adrienne Paton, School of Molecular and Biomedical Science, University of Adelaide, S.A., 5005, Australia (adrienne.paton@adelaide.edu.au).

The Journal of Infectious Diseases 2007; 196:1093–101

0022-1899/2007/19607-0023$15.00

DOI: 10.1086/521364

was among the first STEC serotypes to be causally associated with HUS [4]. The potency of Stx produced by the isolate was comparable to that of typical LEE-positive, HUS-associated strains [3]. We therefore postulated that O113:H21 strains produce an additional cytotoxin capable of augmenting the effects of Stx2 or causing additional pathology. This led to the discovery of subtilase cytotoxin (SubAB), the prototype of a new family of AB_5 toxins, produced by several STEC serotypes [5, 6]. SubAB is more toxic than Stx for Vero cells in vitro and is lethal for mice. It was named "subtilase cytotoxin" because its A subunit (SubA) shares sequence homology with a subtilase-like serine protease of *Bacillus anthracis* [5]. Subtilases are found in a wide variety of microorganisms, but none had previously been shown to be cytotoxic [7]. Mutagenesis of a critical Ser residue in SubA abolished toxicity, which indicates that serine protease activity is central to its mechanism of action [5]. The B subunit is related to putative exported proteins from *Yersinia pestis* and *Salmonella* typhi and binds to glycolipid receptors on target cells [5].

Recently, we reported that the extreme cytotoxicity of SubAB for eukaryotic cells is due to a specific single-site cleavage of the ER chaperone BiP [8]. Structural analysis of SubA revealed an unusually deep active site cleft, which accounted for this exquisite substrate specificity [8]. BiP is a master regulator of ER function [9], and its cleavage represented a previously unknown cytotoxic mechanism. Notwithstanding the extraordinary cytotoxicity of SubAB, its role in the pathogenesis of STEC disease in humans is uncertain. In the present study, we have examined the effects of the administration of purified SubAB to mice. We have found evidence of histopathologic, biochemical, and hematologic changes with striking similarities to those seen in humans with HUS.

MATERIALS AND METHODS

Toxin purification. SubAB and its nontoxic derivative $SubA_{A272}B$ were purified as described elsewhere [5, 10].

Mice. Animal experimentation was approved by the Animal Ethics Committee of the University of Adelaide. Male BALB/c mice, 5–6 weeks old, were injected intraperitoneally (ip) with 5 μg of purified SubAB or $SubA_{A272}B$ (dissolved in 200 μL of PBS). Control mice received 200 μL of PBS.

Biochemical and hematologic analysis. At various times after SubAB injection, mice were anesthetized with Halothane (Veterinary Companies of Australia). Blood samples were obtained via cardiac puncture and collected into either lithium heparin or EDTA tubes. Blood urea, alanine aminotransferase (ALT), aspartate aminotransferase (AST), creatine phosphokinase (CPK), and lactate dehydrogenase (LDH) levels were assayed at Gribbles Veterinary Pathology Laboratory (Adelaide, Australia). Blood glucose levels were measured using a Medisense Optium electrode (Abbott Laboratories). Glucose and protein concentrations in urine were estimated using UriScan dipsticks (YD Diagnostics).

For platelet counts, blood was diluted 1:100 in PBS, and platelets were enumerated by light microscopy. For white blood cell counts, blood in EDTA was diluted 1:20 in acetic blue solution, and cells were counted. Blood smears from 5 μL of blood in EDTA were fixed in 100% methanol for 2 min, stained in Giemsa stain for 4 min, and examined by light microscopy (Axiophot) with an Image Capturing Camera (FUJIX HC-1000, 3CCD; FUJIFILM); digital images were captured and processed using Photograb SP-MA software (version 2.0; FUJIFILM).

Hemolysis and red blood cell (RBC) fragility. For the detection of intravascular hemolysis, plasma hemoglobin concentrations were measured at 6, 24, 48, and 72 h after SubAB injection. Heparinized cardiac blood was diluted 1:100 in isotonic saline and centrifuged at 1500 *g* at 4°C for 10 min, and the A_{540} of the supernatant was measured.

To compare RBC fragility, resistance to hypotonic shock was measured. Heparinized cardiac blood was diluted 1:100 in saline solutions ranging from 2 to 9 g of NaCl per liter. After 30 min at room temperature, suspensions were centrifuged, and the supernatant A_{540} was measured.

Histopathologic analysis. After blood sampling, brain, heart, liver, spleen, and kidneys were removed and fixed in 4% formaldehyde overnight at 4°C, embedded in paraffin, sectioned, stained with hematoxylin-eosin (HE), and examined by light microscopy.

Neutrophil infiltration. Organs—including brain, liver, spleen, kidneys, and ileum—were removed 24 and 48 h after SubAB injection and embedded in OCT Tissue-Tek (Sakura), snap frozen in isopentane cooled with liquid nitrogen, and stored at −80°C. Serial 6-μm sections were cut in a cryostat, air dried, and stored dehydrated at −80°C. Cryopreserved sections were fixed in 4% paraformaldehyde for 20 min and washed 3 times with PBS. Sections were then incubated in the dark for 1 h at room temperature with 50 μL of 50 μg/mL monoclonal rat anti–mouse Ly-6G (specific for granulocyte-restricted cell surface protein [mainly neutrophils]; PharMingen 551459; BD Biosciences) followed by 50 μL of fluorescein isothiocyanate–conjugated donkey anti–rat immunoglobulin (diluted 1:50; Jackson ImmunoResearch). Both antibodies were diluted in 10% heat-inactivated fetal calf serum in PBS. Three PBS washes were performed after each incubation, and slides were examined by fluorescence microscopy.

TUNEL labeling of tissue sections. Apoptosis was assessed by TUNEL labeling using an In Situ Cell Death Detection Kit (Roche) with tetramethylrhodamine red–conjugated nucleotides and terminal deoxynucleotidyl transferase. Cryopreserved sections were fixed in 4% paraformaldehyde for 20 min and permeabilized with 0.1% Triton X-100 and 0.1% sodium citrate in PBS for 2 min at room temperature. Sections were washed

twice with PBS before and after permeabilization. Fifty microliters of TUNEL reagent was added, and sections were incubated in a humidified atmosphere in the dark for 1 h, washed 3 times in PBS, and analyzed by fluorescence microscopy.

Fluorescence microscopy. Fluorescent-labeled tissue sections were mounted in 10 μL of 30% glycerol and analyzed by fluorescence microscopy (AX 70; Olympus); digital images were taken with a Precision Digital Imaging System (Digital Optics). For quantitative analysis, Ly-6G– or TUNEL-positive cells were counted in at least 3 high- or low-power fields.

Statistical analysis. Statistical analysis was performed using Prism software (version 3.03; GraphPad). Data are presented as mean ± SE, and differences were analyzed using Student's *t* test.

RESULTS

Biochemical analysis. Because the tissues targeted by SubAB in vivo have not been determined, blood collected 6, 24, 48 and 72 h after the ip injection of 5 μg of SubAB was analyzed for biochemical markers of specific organ damage. We observed progressive increases in urea, ALT, AST, CPK, and LDH levels in toxin-treated mice (figure 1). For urea levels, the elevation relative to levels of control mice was statistically significant as early as 24 h after injection, whereas for AST, CPK, and LDH levels, statistically significant increases were evident at 48 h. Levels of ALT in blood at 72 h after injection were also elevated but did not reach statistical significance. The elevated urea levels suggest that renal function is impaired within 24 h and that, by 48 h, there is significant damage to other organs, including the liver, as indicated by elevated AST (and possibly ALT) levels. The significant elevation in CPK levels at 48 h is suggestive of myocardial injury, whereas elevated LDH and AST levels may also indicate more generalized toxicity, perhaps including hemolysis. SubAB treatment also caused significant hypoglycemia, with blood glucose levels dropping from 6.95 ± 0.21 mmol/L before injection to 3.55 ± 0.35 and 2.6 ± 0 mmol/L at 24 and 48 h after injection, respectively ($P < .05$ vs. control in both cases). Analysis of urine from toxin-treated mice did not reveal evidence of glucosuria either before or up to 48 h after injection. However, SubAB induced significant proteinuria; urinary protein levels were in the range of 0.3–1 g/L for all mice at both 24 and 48 h after injection, compared with <0.1 g/L before injection.

Histopathologic analysis. Organs—including brain, heart, liver, kidney, and spleen—were subjected to routine histologic examination (HE staining) at 24, 48, and 72 h after SubAB injection. Although there was no obvious damage to cardiac tissue, significant pathologic changes were found in brain, liver, kidney, and spleen (figures 2 and 3). Microvascular thrombosis appeared in the cerebrum (result not shown), brain stem, and cerebellum as early as 24 h after injection (figure 2*B* and 2*E*).

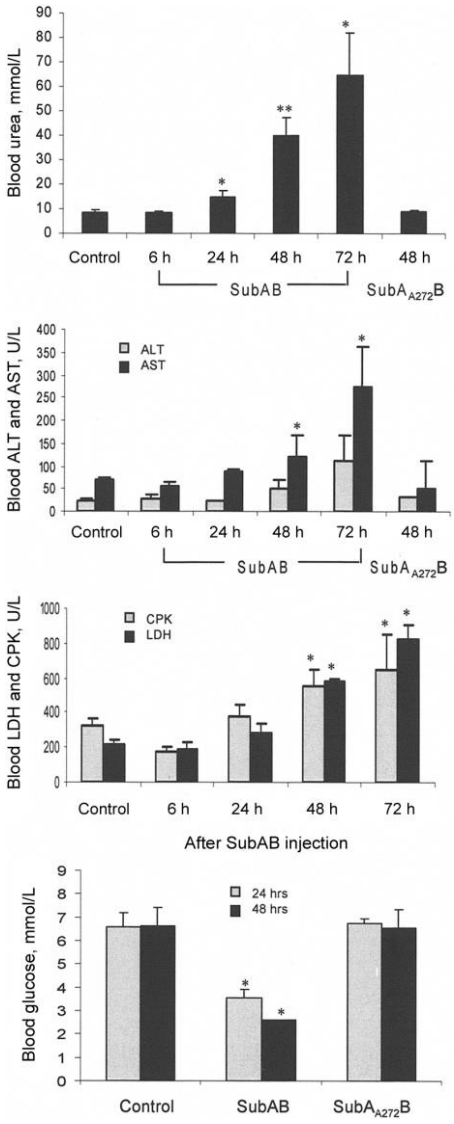

Figure 1. Effect of subtilase cytotoxin (SubAB) on blood chemistry. Blood was collected from control or treated mice at the indicated times after the intraperitoneal injection of 5 μg of SubAB or 5 μg of nontoxic SubA$_{A272}$B ($n = 4$ for each group). Differences between control and toxin-treated mice were analyzed using Student's *t* test: *$P < .05$; **$P < .01$. ALT, alanine aminotransferase; AST, aspartate aminotransferase; CPK, creatine phosphokinase; LDH, lactate dehydrogenase.

At 72 h, microvascular thrombosis was more widespread, and hemorrhagic foci were found in the brain stem and cerebellum (figure 2*C* and 2*F*). Such damage to the brain stem is the likely cause of the sudden death typically observed in mice 3–4 days after the administration of this dose of toxin. The lesions in the cerebellum might also explain the ataxia and uncoordinated movement typically observed immediately before death.

Renal glomeruli were congested from 24 h after SubAB injection, and, at 72 h, some of them exhibited extensive microthrombotic angiopathy and necrotic thrombosis. Renal tu-

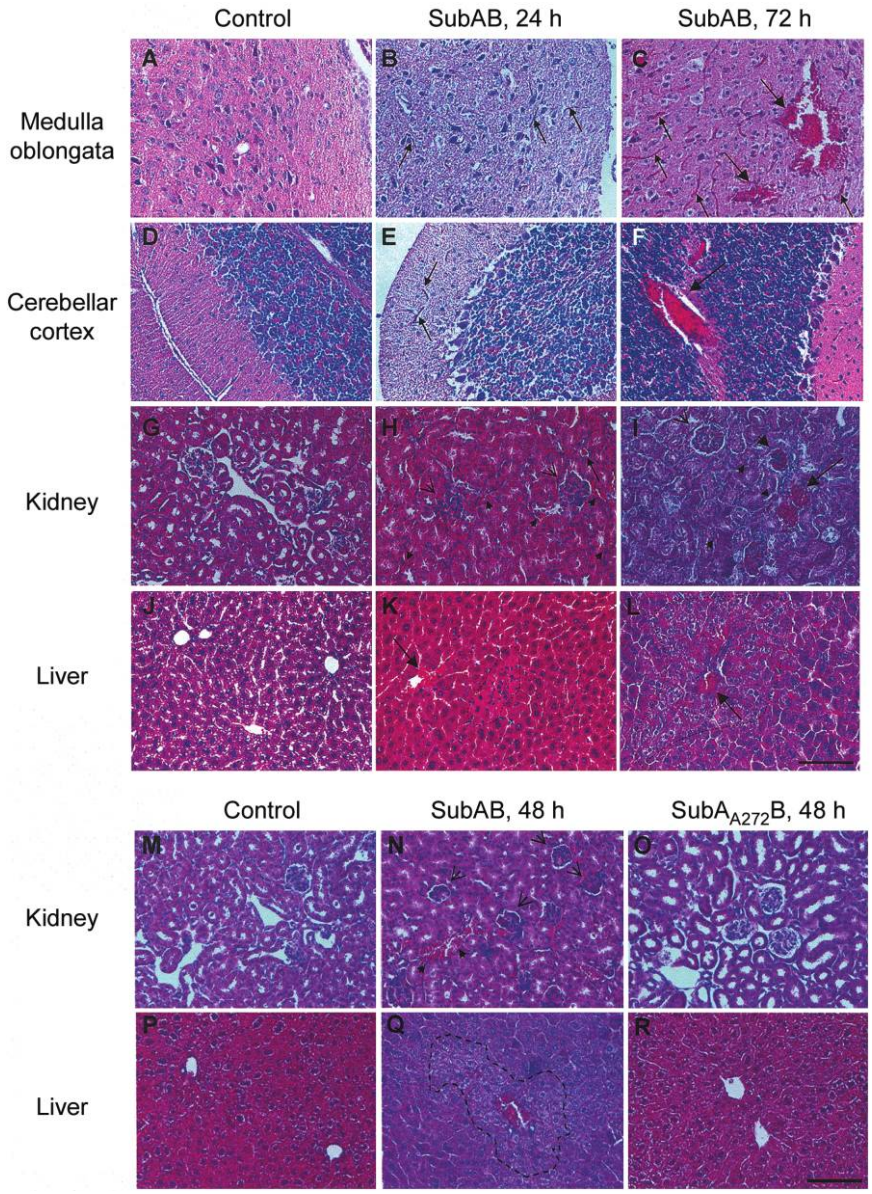

Figure 2. Hematoxylin-eosin (HE)–stained tissue sections of brain stem, cerebellum, kidney, and liver from control and subtilase cytotoxin (SubAB)–treated mice. Extensive microthrombi are evident in the medulla oblongata and cerebellar cortex at both 24 and 72 h after toxin treatment (*small arrows* in panels B, C, and E), with hemorrhagic foci present at 72 h (*large arrows* in panels C and F). The renal cortex also contained microthrombi *(small arrows)* and interstitial hemorrhages *(small arrowheads),* and glomeruli were congested *(open arrowheads)* at 24 and 72 h after SubAB injection (*H* and *I*). At 72 h, capillary lumina were frequently obstructed because of microthrombotic angiopathy (*large arrowhead* in panel I) and necrotic thrombosis (*large arrow* in panel I). Renal tubular epithelial cells were also swollen with diminished lumen diameter, and many were undergoing necrotic change (*H* and *I*). Hepatocytes were swollen, and there were localized necrotic foci *(circled)* at 24 h after SubAB injection. Extensive microthrombi and hemorrhagic foci were found at 72 h *(large arrows)* (*K* and *L*). In an additional experiment, liver and kidney tissue was examined 48 h after treatment with either SubAB (*N* and *Q*) or 5 μg of nontoxic SubA$_{A272}$B (*O* and *R*). Although pathologic findings for the active toxin-treated samples were similar to those observed above, sections from SubA$_{A272}$B-treated mice were indistinguishable from those from untreated controls (*M* and *P*). Scale bar, 0.1 mm.

bules showed extensive epithelial swelling, with decreased lumen space and generalized necrotic changes. Extensive interstitial hemorrhage was seen in the renal cortex from 24 h after SubAB injection (figure 2*H* and 2*I*).

In the liver, hepatocytes were swollen with decreased sinusoidal spaces, and widely distributed necrotic foci were seen as early as 24 h. Extensive microthrombi and hemorrhagic foci were found at 72 h (figure 2*K* and 2*L*).

Macroscopically, there was a dramatic reduction in the size of the spleen, which by 72 h had diminished to only one third

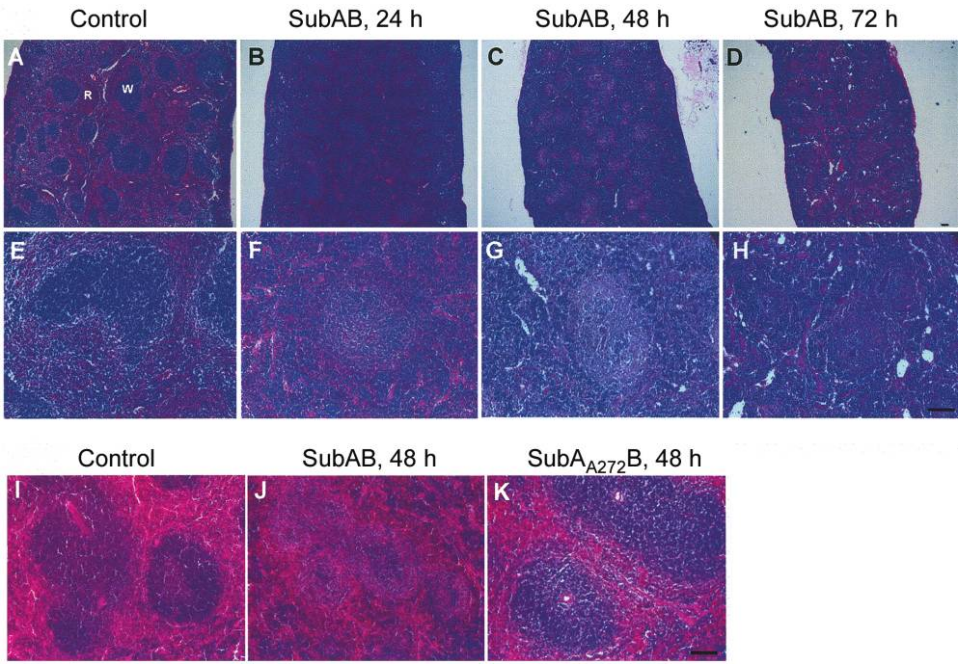

Figure 3. Hematoxylin-eosin (HE)–stained spleen sections from control and subtilase cytotoxin (SubAB)–treated mice at low-power *(top panels)* and high-power *(bottom panels)* magnifications. *B–D, F–H,* Extensive leukocyte redistribution after SubAB injection, compared with normal control spleen tissue (*A* and *E*). Leukocytes disappeared from white pulp and infiltrated the red pulp from 24 h after injection. *A–D,* Significant and progressive decrease in overall size of the spleen after SubAB injection. In an additional experiment, spleens were examined 48 h after treatment with either SubAB *(J)* or 5 μg of nontoxic SubA$_{A272}$B *(K),* with the latter being indistinguishable from the untreated control *(I).* Scale bars, 0.1 mm.

its normal size (figure 3*A*–3*D*), suggesting extensive splenic necrosis. Microscopically, there was marked leukocyte redistribution; leukocytes disappeared from white pulp and infiltrated the red pulp from 24 h after injection (figure 3*E*–3*H*).

Hematologic findings. Examination of Giemsa-stained blood smears (figure 4) indicated that, by 48 h after injection, many of the erythrocytes were fragmented. Platelets were significantly decreased in number, and leukocytes (mainly neutrophils and lymphocytes) appeared to be apoptotic or necrotic. Measurement of free hemoglobin revealed evidence of intravascular hemolysis in 1 of 3 mice tested at 48 h and in 3 of 4 mice tested at 72 h (figure 5*A*). However, erythrocyte osmotic fragility was unaffected by toxin treatment (data not shown), which suggests that intravascular hemolysis was a consequence of physical damage due to microangiopathy rather than a direct effect of the toxin on the erythrocyte membrane.

SubAB injection induced a dramatic decrease in the numbers of platelets in peripheral blood (figure 5*B*). Thrombocytopenia was statistically significant within 6 h of injection, and, by 72 h, platelet counts were <35% of those in normal control mice. SubAB also induced a significant increase in peripheral blood leukocytes at 24 h (figure 5*C*).

Neutrophil infiltration. Neutrophil infiltration was examined in brain, liver, spleen, kidneys, and ileum. Significant infiltration was seen in liver tissue at 24 h after SubAB injection and was even more obvious at 48 h (figure 6*A*). Mean numbers of Ly-6G–positive cells per low-power field had increased 2.9- and 7.7-fold, respectively, at these time points (figure 6*B*) ($P < .01$ in both cases). In the spleen, neutrophil infiltration

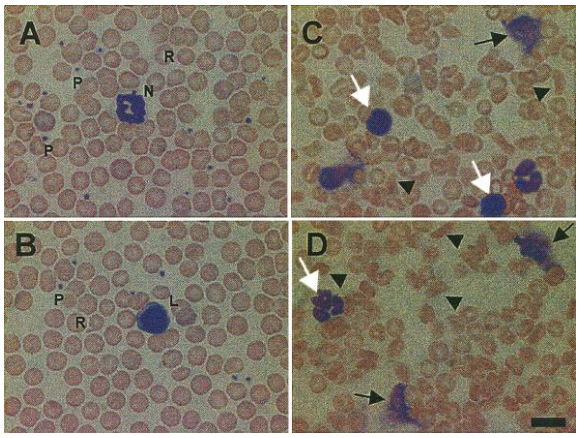

Figure 4. Giemsa-stained blood smears. *A* and *B,* Control mouse. *C* and *D,* Mouse 48 h after subtilase cytotoxin (SubAB) injection. Normal erythrocytes (R), platelets (P), neutrophils (N), and lymphocytes (L) are shown in panels A and B. In panels C and D, platelet nos. were diminished, some of the erythrocytes were fragmented *(arrowheads),* and leukocytes exhibited necrotic *(black arrows)* or apoptotic *(white arrows)* changes. Scale bar, 0.01 mm.

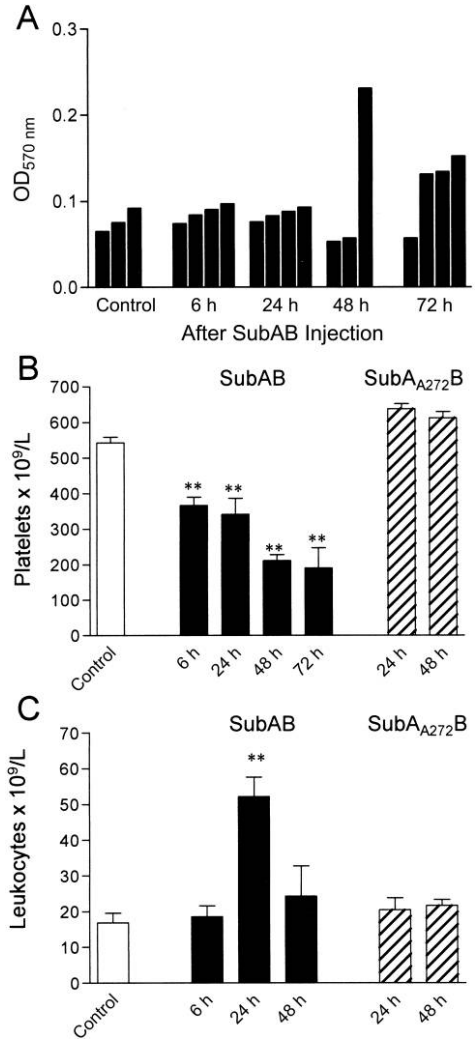

Figure 5. Effect of subtilase cytotoxin (SubAB) on plasma free hemoglobin, platelet, and total leukocyte counts. Blood was collected from control mice and at various times after injection with 5 μg of SubAB. Blood was tested for free hemoglobin ($OD_{570\ nm}$) *(A)* and counted for platelets *(B)* and total leukocytes *(C)*. In panel A, data are shown for each mouse; data for panels B and C are mean ± SE ($n = 4$) for each group. Panels B and C also show data for mice treated with 5 μg of nontoxic $SubA_{A272}B$ *(hatched bars)*. Differences between control and toxin-treated mice were analyzed using Student's *t* test. *$P < .05$; **$P < .01$.

started from the marginal zone of the white pulp at 24 h and extended into the white pulp by 48 h (figure 6*A*). At this time, the total number of Ly-6G–positive cells had increased by ~65% (figure 6*B*) ($P < .05$). In the kidney, neutrophil infiltration appeared to peak at 24 h after SubAB injection (figure 6*A*). Numbers of Ly-6G–positive cells were 5.5- and 2.9-fold higher than those of control tissue at 24 and 48 h, respectively (figure 6*B*) ($P < .05$ and $P < .01$, respectively). Significant infiltration was not observed in either the brain or the ileum (data not shown).

Apoptosis. Induction of apoptosis in tissues by SubAB was assessed using the TUNEL assay (figure 7). In the spleen, increased TUNEL-positive leukocyte counts (mainly lymphocytes and neutrophils) were seen at 24 h after injection, relative to numbers in control mice. Mean numbers of TUNEL-positive cells per high-power field were 41.4 ± 7.3 and 6.25 ± 1.28, respectively ($P < .01$). In the kidney, increased tubule apoptosis was apparent at 48 h, with 8.5 ± 1.26 TUNEL-positive cells per low-power field, compared with 3.0 ± 0.47 for control tissue ($P < .01$). In the liver, increased numbers of TUNEL-positive hepatocytes were seen at 24 h (13.7 ± 1.48 per low-power field, compared with 3.0 ± 0.94 for control tissue; $P < .01$).

Experiments using a nontoxic SubAB derivative. The SubAB used in these studies was purified from recombinant *E. coli;* therefore, some of the observed effects might be due to contamination with lipopolysaccharide (LPS). Additional mice were therefore injected ip with 5 μg of a mutant derivative of SubAB (designated $SubA_{A272}B$) that had been purified using an identical protocol. $SubA_{A272}B$ has a Ser_{272}→Ala mutation in the A subunit that completely abolishes serine protease activity and cytotoxicity for Vero cells [5, 10]. Leukocyte and platelet numbers were monitored in tail blood before and 24 or 48 h after injection (figure 5*B* and 5*C*). Blood urea, ALT, AST, glucose (figure 1), urine glucose, and protein (data not shown) levels and histopathologic features (figures 2*M*–2*R* and 3*I*–3*K*) were examined at 48 h. There was no detectable difference between $SubA_{A272}B$-treated mice and untreated mice for any of these parameters. Therefore, the pathology induced by ip injection of active SubAB is not due to LPS contamination and is directly attributable to the serine protease activity of the A subunit of the toxin.

DISCUSSION

SubAB is a potentially important bacterial virulence factor, although assessment of its contribution to pathogenesis is complicated, because the strains of *E. coli* shown thus far to produce it also produce Stx [5, 6]. Both toxins are highly potent for Vero cells, but their glycolipid receptor specificities and mechanisms of action are distinct [3, 5, 8]. Thus, the tissues affected by the 2 toxins in vivo will be determined by their expression of the respective receptors, whereas the biochemical properties of the respective A subunits will determine the nature of cellular damage. To our knowledge, this is the first systematic study of the in vivo effects of purified SubAB in a mouse model, which will inform future examination of the role of this emerging toxin in human disease. Toxin was administered ip, because it would be expected to enter the portal circulation, as would toxin absorbed from the gut during a natural infection with SubAB-producing STEC, thereby modeling potential systemic effects of the toxin.

Remarkably, many of the in vivo effects observed in SubAB-treated mice parallel those seen in human cases of STEC-associated HUS [11, 12] and in animals injected with purified

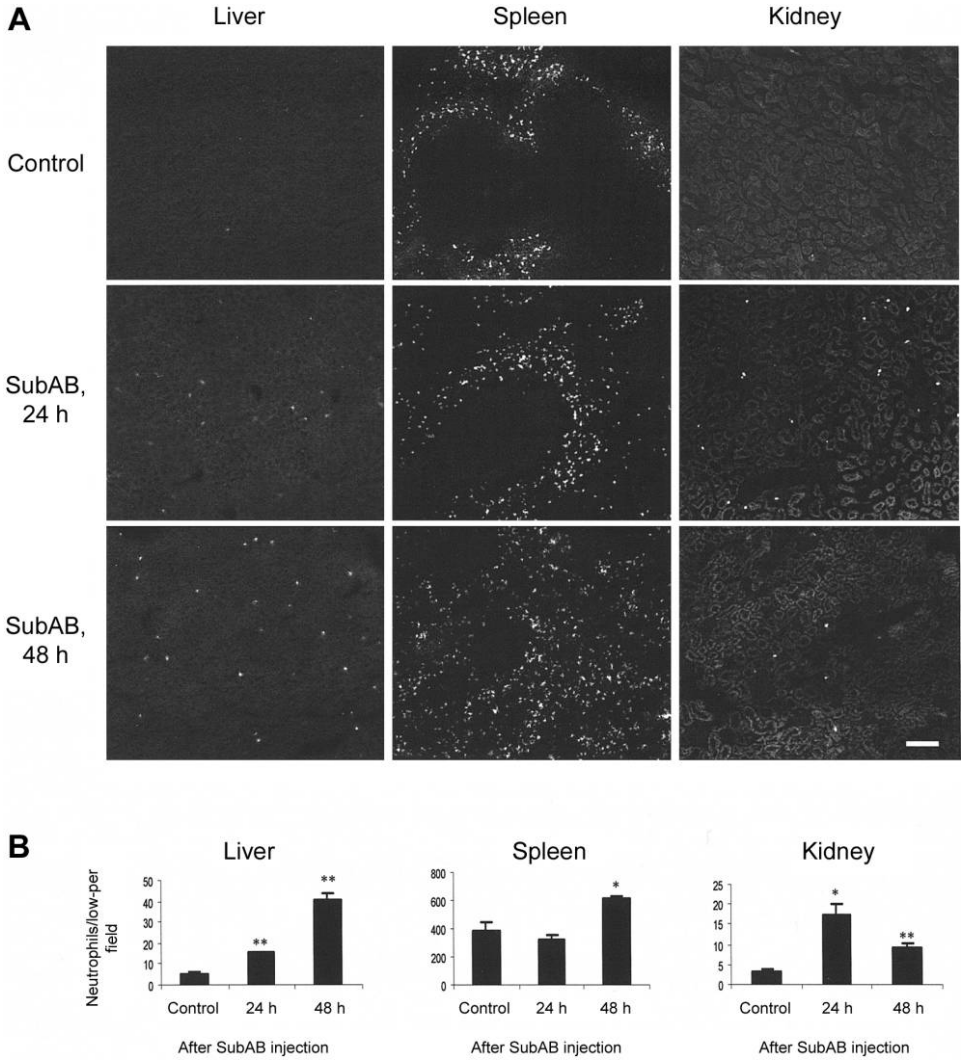

Figure 6. Neutrophil infiltration. Cryopreserved sections of liver, spleen, and kidney tissue from control and subtilase cytotoxin (SubAB)–treated mice (24 or 48 h after injection) were stained using immunofluorescence for the neutrophil surface marker Ly-6G *(A).* Scale bar, 1 mm. Ly-6G–positive cells were also counted in at least 3 low-power fields *(B).* Data are mean ± SE; differences between control and toxin-treated mice were analyzed using Student's *t* test. $^{*}P < .05$; $^{**}P < .01$.

Stx [13–15]. Hematologically, there was evidence of microangiopathic hemolytic anemia, thrombocytopenia, and leukocytosis. Biochemical analysis revealed elevated plasma urea levels, indicating renal impairment. Histologic examination showed extensive renal damage, including swollen and congested glomeruli and tubular epithelial cells, extensive thrombotic microangiopathy, generalized necrotic changes, and interstitial hemorrhages. There was also evidence of neutrophil infiltration into the kidney and induction of tubular apoptosis. In the brain, there was extensive microvascular thrombosis in the cerebrum, brain stem, and cerebellum, with hemorrhagic foci in the latter 2 sites. These findings raise the possibility that Stx may not be entirely responsible for the life-threatening systemic sequelae of gastrointestinal infections caused by STEC strains producing both toxins. Clearly, it will be important to investigate the pathologic effects of delivery of SubAB via the gastrointestinal tract in future studies, in case the presence or absence of receptors in the gut affect toxin uptake and trafficking. Interestingly, however, in mouse models, Stx administered systemically causes pathology more like that seen in human HUS than does Stx produced in situ by bacteria in the gut [1].

Notwithstanding the striking overlap between the pathology induced by the 2 distinct toxins, SubAB elicited several additional changes that, to our knowledge, have not been previously ascribed to Stx, either in humans or in animal models. Most notable was the profound damage to the liver, including swollen hepatocytes, decreased sinusoidal spaces, extensive microthrombi and hemorrhagic and necrotic foci, recruitment of neutrophils, and evidence of induction of apoptosis, as well as elevated liver enzyme levels in plasma. SubAB treatment also

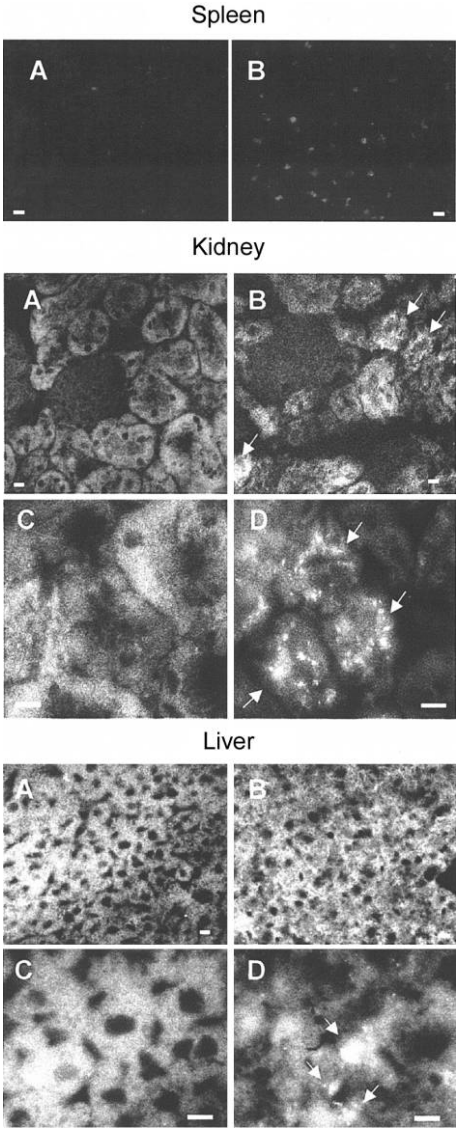

Figure 7. Apoptosis in spleen, kidney, and liver tissue from control and subtilase cytotoxin (SubAB)–treated mice. Apoptosis was assessed by fluorescent TUNEL staining of cryopreserved sections from a control mouse (*A* and *C*) and from SubAB-treated mice (after 24 h for spleen and liver and after 48 h for kidney tissue) (*B* and *D*). Panels A and B are low-power images; panels C and D are high-power images. Arrows indicate TUNEL-positive nuclei. Scale bars, 0.01 mm.

induced profound splenic atrophy and massive redistribution of leukocytes. The white pulp had a hollow appearance, which may have been due to a combination of lymphocyte migration and increased apoptosis or necrosis. HE staining revealed some pyknotic and some karyolitic lymphocyte nuclei, whereas TUNEL staining also revealed increased apoptosis of neutrophils and lymphocytes at 24 h after treatment. Increased apoptotic cells in the spleen have also been reported in mice injected intravenously with Stx1 or Stx2 [16].

Urine analysis also revealed evidence of proteinuria at 24 and 48 h after SubAB treatment, consistent with the renal damage observed histopathologically, but glucosuria was not detected. By contrast, Rutjes et al. [16] reported that mice treated with Stx do exhibit glucosuria, albeit at later time points than those used here, but proteinuria was not detected. As we have recently reported [8], the mechanism of action of SubAB involves specific cleavage of the essential ER chaperone BiP. BiP's functions include mediating the correct folding of nascent secretory proteins, maintaining the permeability barrier of the ER membrane, and targeting terminally misfolded proteins to the Sec61 apparatus for retrotranslocation into the cytosol and degradation [17, 18]. BiP plays a crucial role in the unfolded protein response as the ER stress-signaling master regulator [9] and exhibits antiapoptotic properties through interference with caspase activation [19–21]. SubAB cleaves BiP at a dileucine motif in the hinge region between the ATPase and protein-binding domains, potentially blocking many of these functions [8]. In Vero cells, this cleavage occurs very rapidly and is complete within 30 min at high toxin doses [8]. Although the downstream effects of BiP cleavage within the cell have yet to be fully investigated, these are likely to include ectopic accumulation of misfolded proteins in the ER lumen, a massive ER stress response, and induction of apoptosis. We have recently detected cleavage of BiP in the livers of mice injected with active SubAB and initiation of an unfolded protein response, as indicated by induction of the transcription factor C/EBP homologous protein at 24 h after injection [8]. In the present study, we have presented evidence of increased apoptosis in the liver, spleen, and kidney at similar times.

The multiple organ damage induced by SubAB could be a consequence of direct effects on tissues or cells due to the blockade of BiP function. This would be dependent on expression of the cognate receptor on the surface of such tissues or cells, enabling uptake of the toxin. Comprehensive investigations of receptor distribution have yet to be conducted for SubAB. Damage to tissues could also be mediated by ischemia/hypoxia due to extensive thrombotic microangiopathy, as well as by inflammation secondary to neutrophil infiltration, as observed in the present study. A complete understanding of in vivo tissue tropism and the mechanism whereby SubAB inflicts organ damage in animal models will inform future investigations of its potential role in human disease. Studies are also required to determine whether SubAB and Stx act in synergy to induce pathology. Also, clinicians need to be aware of the possibility of additional multiorgan complications occurring in patients infected with STEC strains that also produce SubAB. At present, there is little information on the global distribution of such strains. Reference and diagnostic laboratories should be encouraged to test existing strain collections and fresh clinical isolates for the presence of the toxin genes by polymerase chain reaction [6]. To date, the genes encoding this emerging

toxin have been detected only in LEE-negative STEC [5, 6]. However, the genes are located on a self-transmissible megaplasmid [5], raising the possibility of widespread dissemination among diverse *E. coli* host strains or even other Enterobacteriaceae.

References

1. Paton JC, Paton AW. Pathogenesis and diagnosis of Shiga toxin-producing *Escherichia coli* infections. Clin Microbiol Rev **1998**; 11:450–79.
2. Nataro JP, Kaper JB. Diarrheagenic *Escherichia coli.* Clin Microbiol Rev **1998**; 11:142–201.
3. Paton AW, Woodrow MC, Doyle RM, Lanser JA, Paton JC. Molecular characterization of a Shiga-toxigenic *Escherichia coli* O113:H21 strain lacking *eae* responsible for a cluster of cases of hemolytic-uremic syndrome. J Clin Microbiol **1999**; 37:3357–61.
4. Karmali MA, Petric M, Lim C, Fleming PC, Arbus GS, Lior H. The association between idiopathic hemolytic uremic syndrome and infection by verotoxin-producing *Escherichia coli.* J Infect Dis **1985**; 151: 775–82.
5. Paton AW, Srimanote P, Talbot UM, Wang H, Paton JC. A new family of potent AB_5 cytotoxins produced by Shiga toxigenic *Escherichia coli.* J Exp Med **2004**; 200:35–46.
6. Paton AW, Paton JC. Multiplex PCR for direct detection of Shiga toxigenic *Escherichia coli* producing the novel subtilase cytotoxin. J Clin Microbiol **2005**; 43:2944–7.
7. Siezen RJ, Leunissen JAM. Subtilases: the superfamily of subtilisin-like serine proteases. Protein Sci **1997**; 6:501–23.
8. Paton AW, Beddoe T, Thorpe CM, et al. AB_5 subtilase cytotoxin inactivates the endoplasmic reticulum chaperone BiP. Nature **2006**; 443: 548–52.
9. Hendershot LM. The ER chaperone BiP is a master regulator of ER function. Mt Sinai J Med **2004**; 71:289–97.
10. Talbot UM, Paton JC, Paton AW. Protective immunization of mice with an active-site mutant of subtilase cytotoxin of Shiga toxin-producing *Escherichia coli.* Infect Immun **2005**; 73:4432–6.
11. Inward CD, Howie AJ, Fitzpatrick MM, Rafaat F, Milford DV, Taylor CM. Renal histopathology in fatal cases of diarrhoea-associated haemolytic uraemic syndrome. Pediatr Nephrol **1997**; 11:556–9.
12. Proulx F, Seidman EG, Karpman D. Pathogenesis of Shiga toxin-associated hemolytic uremic syndrome. Pediatr Res **2001**; 50:163–71.
13. Richardson SE, Rotman TA, Jay V, et al. Experimental verocytotoxemia in rabbits. Infect Immun **1992**; 60:4154–67.
14. Siegler RL, Obrig TG, Pysher TJ, Tesh VL, Denkers ND, Taylor FB. Response to Shiga toxin 1 and 2 in a baboon model of hemolytic uremic syndrome. Pediatr Nephrol **2003**; 18:92–6.
15. Yamamoto ET, Mizuno M, Nishikawa K, et al. Shiga toxin 1 causes direct renal injury in rats. Infect Immun **2005**; 73:7099–106.
16. Rutjes NWP, Binnington BA, Smith CR, Maloney MD, Lingwood CA. Differential tissue targeting and pathogenesis of verotoxins 1 and 2 in the mouse animal model. Kidney Int **2002**; 62:832–45.
17. Gething MJ. Role and regulation of the ER chaperone BiP. Semin Cell Dev Biol **1999**; 10:465–72.
18. Hamman BD, Hendershot LM, Johnson AE. BiP maintains the permeability barrier of the ER membrane by sealing the lumenal end of the translocon pore before and early in translocation. Cell **1998**; 92: 747–58.
19. Lee AS. The ER chaperone and signaling regulator GRP78/BiP as a monitor of endoplasmic reticulum stress. Methods **2005**; 35:373–81.
20. Rao RV, Ellerby HM, Bredesen DE. Coupling endoplasmic reticulum stress to the cell death program. Cell Death Differ **2004**; 11:372–80.
21. Rao RV, Peel A, Logvinova A, et al. Coupling endoplasmic reticulum stress to the cell death program: role of the ER chaperone GRP78. FEBS Lett **2002**; 514:122–8.